


Article

An Improved Method of Heart Rate Extraction Algorithm Based on Photoplethysmography for Sports Bracelet

Binbin Ren ^{1,2,†}, Zhaoyuxuan Wang ^{1,†}, Kainan Ma ¹ , Yiheng Zhou ¹ and Ming Liu ^{1,3*}

¹ Institute of Semiconductors, Chinese Academy of Sciences, Beijing 100083, China; renbinbin@semi.ac.cn (B.R.); wangzhaoyuxuan@semi.ac.cn (Z.W.); makainan@semi.ac.cn (K.M.); zhouyiheng@semi.ac.cn (Y.Z.)

² School of Electronic, Electrical and Communication Engineering, University of Chinese Academy of Sciences, Beijing 100049, China

³ School of Integrated Circuits, University of Chinese Academy of Sciences, Beijing 100049, China

* Correspondence: liuming@semi.ac.cn

† These authors contributed equally to this work.

Abstract: Heart rate measurement employing photoplethysmography (PPG) is a prevalent technique for wearable devices. However, the acquired PPG signal is often contaminated with motion artifacts, which need to be accurately removed. In cases where the PPG and accelerometer (ACC) spectra overlap at the actual heart rate, traditional discrete Fourier transform (DFT) algorithms fail to compute the heart rate accurately. This study proposed an enhanced heart rate extraction algorithm based on PPG to address the issue of PPG and ACC spectral overlap. The spectral overlap is assessed according to the morphological characteristics of both the PPG and ACC spectra. Upon detecting an overlap, the singular spectrum analysis (SSA) algorithm is employed to calculate the heart rate at the given time. The SSA algorithm effectively resolves the issue of spectral overlap by removing motion artifacts through the elimination of ACC-related time series in the PPG signal. Experimental results reveal that the accuracy of the proposed algorithm surpasses that of the traditional DFT method by 19.01%. The proposed method makes up for the deficiency posed by artifact and heart rate signal overlap in conventional algorithms and significantly improves heart rate extraction accuracy.

Keywords: heart rate extraction; accelerometer; photoplethysmography; discrete Fourier transform; singular spectrum analysis



Citation: Ren, B.; Wang, Z.; Ma, K.; Zhou, Y.; Liu, M. An Improved Method of Heart Rate Extraction Algorithm Based on Photoplethysmography for Sports Bracelet. *Information* **2023**, *14*, 297. <https://doi.org/10.3390/info14050297>

Academic Editor: Alessandra Lumini

Received: 20 April 2023

Revised: 17 May 2023

Accepted: 17 May 2023

Published: 19 May 2023



Copyright: © 2023 by the authors. Licensee MDPI, Basel, Switzerland. This article is an open access article distributed under the terms and conditions of the Creative Commons Attribution (CC BY) license (<https://creativecommons.org/licenses/by/4.0/>).

1. Introduction

As wearable hardware devices continue to advance and people's awareness of health monitoring steadily increases, physiological signal acquisition systems have made considerable progress in terms of portability and domestic usage. Among various parameters, heart rate has emerged as a crucial component for long-term physiological monitoring [1–3]. Heart rate-measurement methods can be broadly classified into two categories, electrocardiograms (ECGs) and photoplethysmography (PPG), with the latter being predominantly employed in daily assessments. PPG, which relies on LED light sources and detectors, measures pulse waves by detecting light attenuation due to reflection and absorption by human blood vessels. The intensity of the light can be utilized to monitor blood volume changes or other alterations within human tissue [2]. Different physiological information can be revealed according to the frequency of the light wave and the sensor used [3]. PPG measurement is widely used in wearable devices such as oximeters, sports bracelets and smartwatches. In these devices, PPG signals are often disrupted by motion artifacts (MAs) stemming from the user's voluntary or involuntary movements [4]. To mitigate the interference of motion artifacts and acquire the cleanest possible PPG signal, accelerometers (ACCs) are employed to measure motion signals. By comparing the PPG and ACC signals, the impact of motion artifacts on heart rate measurement can be effectively reduced [5,6].

PPG-based heart rate extraction algorithms typically consist of the following key steps. First, the PPG signal undergoes preprocessing, which includes band-pass filtering, down-sampling and normalization. Second, motion artifacts are removed, generally by using accelerometer signals as a reference. Commonly employed methods encompass adaptive filtering, independent component analysis, empirical mode decomposition, wavelet decomposition, spectral subtraction and Kalman filtering. Third, the heart rate of clean signals is estimated by analyzing the spectral components of PPG signals after motion artifact removal. It is evident that filtering is widely utilized in PPG preprocessing; however, it may result in waveform distortion. Liu et al. [7] demonstrated that the measurement site and type of pulse feature have a significant influence on the time shift in feature point between the prefiltered and filtered PPG signals. The finger, which is the most commonly used measurement site for PPG signals, exhibits a higher overall time shift. Allen et al. [8] emphasized the importance of a suitable filter to avoid pulse shape distortion. Concurrently, as artificial intelligence advances, deep learning can be employed for preprocessing noise generated by cardiac or respiratory activities. In [9–11], deep learning was introduced for PPG signal preprocessing and feature extraction, with data input into neural networks to assist researchers in auxiliary calculations.

Traditional PPG heart rate algorithms can be broadly classified into two categories: methods based on time-domain features (such as peak number algorithm) and methods based on frequency-domain features (such as discrete Fourier transform, DFT).

Time-domain methods typically involve extracting heart rate information directly from the PPG waveform, often employing a two-stage process. The first stage consists of pre-processing, which filters out disturbances from the PPG signal. The second stage involves heart rate extraction by decomposing the PPG signal, allowing for peak counting within the signal. For instance, Khan et al. proposed a method that initially eliminates runaway errors based on ensemble empirical mode decomposition (EMD), followed by the use of recursive least squares (RLS) filters to further calculate the heart rate [12]. Ye et al. [13] proposed a hybrid motion artifact-removal method, combining nonlinear adaptive filtering and signal decomposition. However, time-domain methods may prove unreliable when motion noise exhibits periodic and robust characteristics, as extracting a clean PPG signal becomes increasingly challenging under such conditions.

Frequency-domain methods compensate for the limitations of time-domain approaches, as periodic disturbances can be more readily removed in the frequency domain than in the time domain. Salehizadeh et al. [5] proposed a technique for accurately reconstructing motion-corrupted PPG signals and heart rate based on time-varying spectral analysis. This approach involves calculating the power spectral density of both PPG and accelerometer signals for each time shift within a windowed data segment. By comparing the time-varying spectra of PPG and accelerometer data, frequency peaks resulting from motion artifacts can be distinguished from the PPG spectrum. Fukushima et al. [14] and Chen et al. [15] suggested a spectrum subtraction technique to remove the acceleration data spectrum from the PPG signal. However, frequency domain methods may exhibit limited effectiveness in the presence of irregular or aperiodic disturbances, such as complex hand movements encountered while ascending and descending stairs. Under such conditions, complex methods are often employed, although they generally exhibit high computational complexity. Salehizadeh et al. [16] proposed a motion artifact-removal algorithm using Singular Spectrum Analysis (SSA). They utilized SSA to decompose the corrupted segment adjacent to the clean segment and selected the SSA components in the corrupted segment with a frequency range similar to the clean adjacent components. Despite their effectiveness, algorithms based on complex feature extraction tend to have high computational complexity and lengthy operation times, rendering them unsuitable for long-term use in wearable devices that require continuous heart rate detection.

In our experiments, the accuracy of heart rate estimation for some samples was found to be relatively low. This may be attributed to several factors. First, noise could have been introduced due to changes in the distance between the measurement site and the testing

equipment during physical activity. Second, higher harmonics of respiratory modulations in frequency, amplitude and baseline [17], as well as neural activities, may have confounded the results [18,19]. Additionally, we observed that when the low-frequency component in the ACC signal is similar to the heart rate, the peak corresponding to the actual heart rate in the PPG spectrum is subtracted as a motion artifact, causing the algorithm to yield a value significantly higher than the actual heart rate. This phenomenon occurs during activities with substantial movement but relatively low heart rate, such as walking up and down stairs. Upon reviewing the literature, we found that this issue has not been previously addressed.

To solve the issue caused by the overlap of the PPG and ACC spectra at the actual heart rate, we propose an improved algorithm framework for PPG-based heart rate measurement. First, we judge whether there is spectral overlap between the PPG spectrum and the ACC spectrum. If such overlap exists, we employ the Singular Spectrum Analysis (SSA) algorithm to remove the time series related to ACC in PPG signal. Subsequently, the PPG signal is processed using DFT and peak search, culminating in the calculation of the heart rate. This algorithm eliminates the need to subtract the PPG spectrum from the ACC spectrum signal in the frequency domain, allowing for accurate heart rate calculation even in cases of spectral overlap. In conjunction with experimental measurements, the accuracy of the improved algorithm for heart rate calculation is enhanced by at least 19.01% compared to the traditional DFT method.

The rest of this paper is organized as follows: Section 2 introduces the experimental equipment, experimental objects, traditional algorithm process and experiment results; Section 3 introduces the improved algorithm process and experiment results; Section 4 discusses the comparison between the improved algorithm and the original algorithm; and Section 5 draws conclusions.

2. Materials and Methods

2.1. Experimental Equipment and Objects

In this study, the experimental setup comprised two bracelets, two Polar H10 heart rate bands and two Android phones with Bluetooth functionality. The bracelets were equipped with a green LED sensor and a photodiode (PD) that converted light energy into electrical signals to collect PPG signals, as well as a LIS2DH12 sensor (STMicroelectronics, Geneva, Switzerland.) for capturing acceleration data. The Polar H10 heart rate band (Polar, Kempele, Finland.) was employed to monitor participants' real-time ECG signals, which, after processing, served as a standard for heart rate comparison. The mobile phone received heart rate information from the Polar H10 heart rate band. Figure 1 shows the heart rate band and bracelet being worn. Figure 2 shows the participants in the experiment.

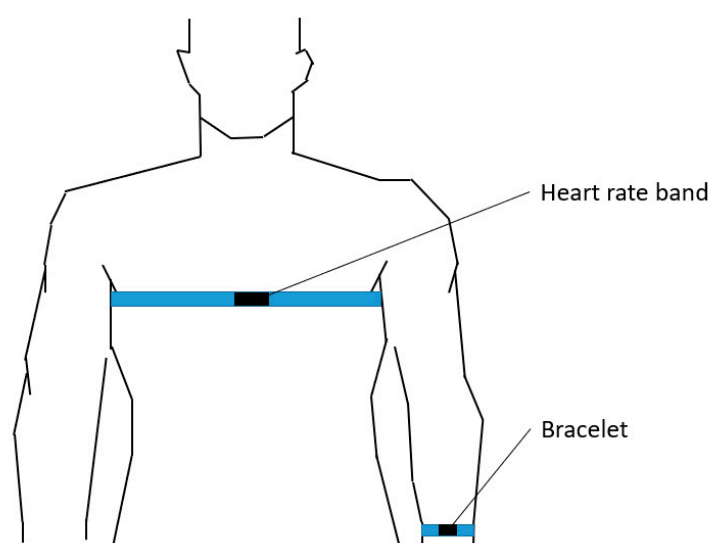


Figure 1. Heart rate band and bracelet being worn.

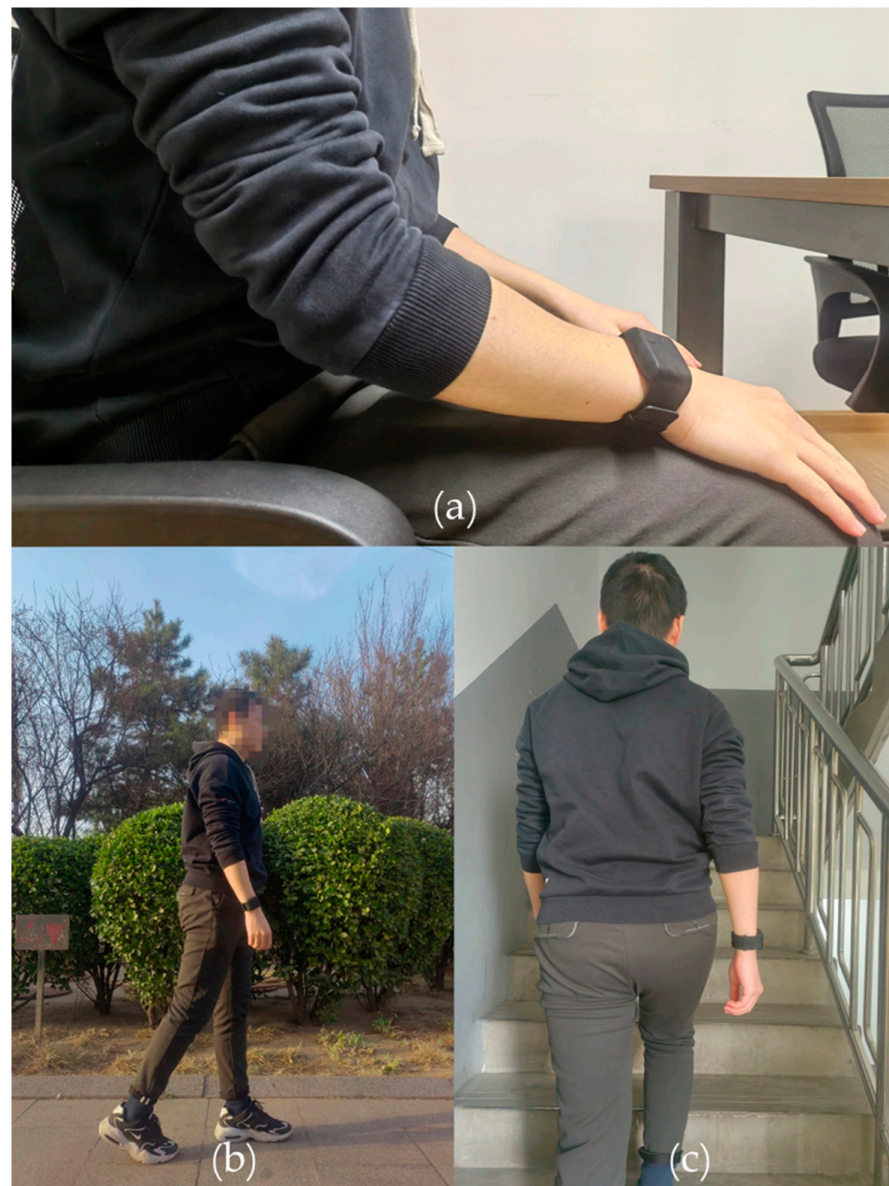


Figure 2. Pictures of participants during the experiment. (a) Sitting; (b) Outdoor walking; (c) Walking up and down stairs.

This experiment involved 20 participants, comprising 11 males and 9 females, all of Asian descent and residing in China. Their ages ranged from 24 to 32 years old, with male participants' heights varying between 165 and 185 cm, and female participants' heights between 155 and 170 cm. The average age was 26.35 years, with a standard deviation of 1.93, while the average height was 168.55 cm, with a standard deviation of 7.81. The experimental setting was an office building within a research institute. The experimental process included sitting, daily activities, walking up and down stairs, outdoor walking and outdoor jogging. In order to mitigate the impact of experimental equipment on the results of the study, two sets of experimental equipment were utilized. This approach ensured that the performance of the algorithm was not reliant on the specific hardware employed during testing. The experimental procedures and standards were modeled after those used for commercial bracelets. Table 1 displays the test protocol and experimental procedure used for data collection.

Table 1. Test protocol and experimental procedure of data collection.

Experimental Items	Preconditions	Experimental Procedure	Judgment Standard
Sitting	Participants were instructed to remain calm for at least 2 min prior to the experiment, commencing with a low heart rate of 100 bpm.	The participant places their hands on their thighs and sits quietly on a chair for a duration of 10 min.	When comparing with the heart rate measured by the heart rate band, sample values exhibiting an estimated heart rate deviation within ± 10 bpm are considered accurate.
Daily activities	The same as above.	<ol style="list-style-type: none"> 1. The participant takes a seat on the chair in front of the computer; 2. Repeatedly types the phrase “Midsummer Night Dream” for a duration of 2 min using the keyboard; 3. Utilizes the arm wearing the bracelet to pick up and put down a pen 20 times within a 1 min timeframe; 4. Unties and ties their shoelace 10 times within a 2 min period. 	The same as above.
Walking up and down stairs	The same as above.	<p>The participant proceeds to walk up and down the stairs at a slow pace, ensuring that the effective experimental duration extends beyond 10 min.</p> <p>The participant walks at a comfortable pace, typically on a flat, non-sloping surface during a sunny day, allowing both arms to swing naturally, and maintains this movement for a duration of 10 min.</p>	The same as above.
Outdoor walking	The same as above.	<p>The participant engages in running on a flat, non-sloping surface during a sunny day, with the effective experimental duration lasting for more than 10 min.</p>	The same as above.
Outdoor jogging	The same as above.		The same as above.

Participants were instructed to wear both the Polar H10 heart rate band and the bracelet, ensuring that the bracelet was positioned close to the wrist and away from the wrist bone. They were asked to follow the test preconditions in Table 1 to rest for at least 2 min to guarantee that their initial heart rate corresponded to their resting heart rate before they started the test projects. After the experiment, the estimated heart rate measured by the bracelet was compared with that measured by the Polar H10 heart rate band. The experiment consisted of 20 participants, each of whom participated in all 5 test projects. Each activity project is considered as a set, consisting of 20 samples. The heart rate band calculated heart rate once per second, so each sample consisted of 300 or 600 heart rate values, depending on the experimental duration. An estimated heart rate was considered accurate if the difference from the true heart rate was no more than ± 10 bpm, and a sample was considered qualified if over 90% of the estimated heart rates were accurate.

2.2. Traditional Algorithm Architecture

The traditional PPG heart rate extraction algorithm based on Discrete Fourier Transform (DFT) primarily consists of three components: baseline drift removal, discrete Fourier transform and motion artifact elimination. The algorithm architecture is depicted in Figure 3. At present, optical heart rate sensors are predominantly worn in the following positions: the ear, arm, wrist and finger [20,21]. Earlobe-based PPG sensors are less

susceptible to motion artifacts than wrist-based sensors and provide a more accurate measurement of PPG signals. However, they may not be as convenient to wear and may require a tighter fit to the ear to reduce the effects of motion. The arm presents a good location for PPG measurement, due to its good blood perfusion and relative insensitivity to motion. Yet, it may be more challenging to access and may not offer the most precise measurement of PPG signals. The fingertip is a good location for PPG measurement because it has good blood perfusion and is relatively insensitive to motion. However, the fingertip may be more sensitive to changes in temperature and may not provide the most accurate measurement of PPG signals. Wrist-worn PPG sensors, despite being convenient and accessible, may not provide the most accurate measurement of PPG signals, as the wrist is more susceptible to motion artifacts. The measurement location or placement of an accelerometer is crucial for obtaining accurate and reliable data [22]. Depending on the application, accelerometers can be placed on various body parts. In summary, for the purpose of developing smart sports bracelets, the wrist was selected as the measurement site for this study's algorithm.

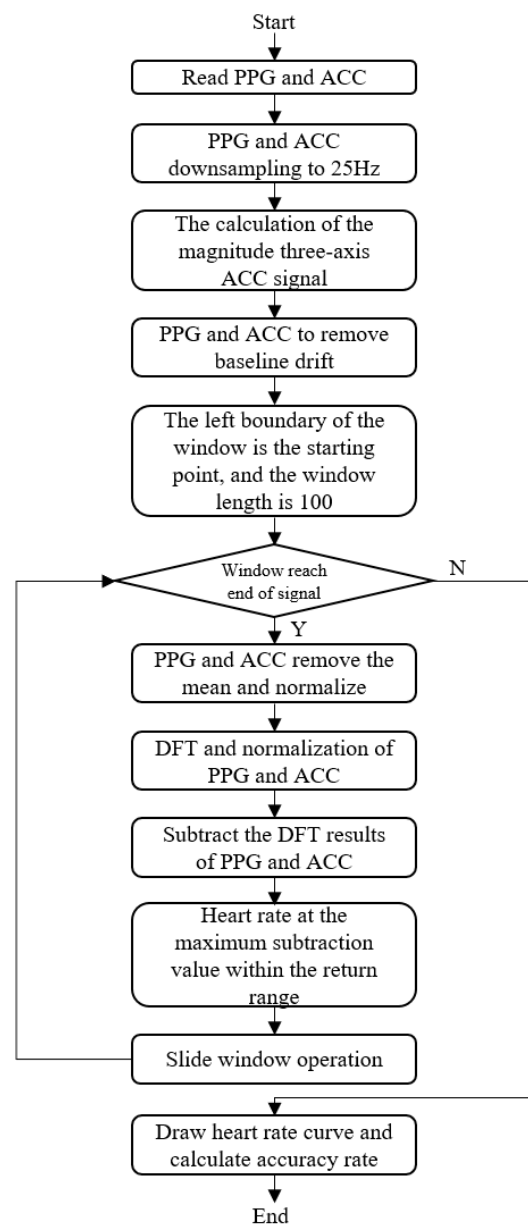


Figure 3. Traditional algorithm architecture diagram.

First, the bracelet was used to collect the participant's PPG and ACC signals. In this study, a mean filter was utilized to effectively mitigate baseline drift. Initially, the raw signal was introduced into a mean filter featuring a window length of 7, following which the output of the mean filter was subtracted from the original signal to derive the signal with the mean value removed. Subsequently, the resultant signal was channeled into an additional mean filter possessing a window length of 3. The output signal generated in this stage represents the final signal, successfully devoid of baseline drift. Then the ACC was used to eliminate the motion artifact present in the PPG signal. Baseline drift is typically caused by noise with a frequency below 1 Hz, generated by human respiration and friction between the skin surface and the PPG signal acquisition equipment. This noise manifests as a low-frequency curve superimposed on the original signal, causing the signal to fluctuate over time [23]. Based on the definition of baseline drift, high-pass filtering can be employed to filter out noise below 1 Hz, effectively removing the baseline drift. In order to reduce computational complexity, baseline drift is removed by subtracting the mean-filtered signal from the original signal.

Utilizing a sliding window approach for heart rate calculation, increased window lengths offer enhanced noise resistance and produce smoother heart rate signal curves, albeit at the expense of greater computational demands. In contrast, shorter window lengths present the inverse effects. To maintain the algorithm's robustness without substantially raising computational requirements, we opted for a window length of 100 data points. PPG and ACC signals were downsampled to 25 Hz, and heart rate was calculated once per second. Therefore, the length of the sliding window was set to 25 data points. These parameters could be adjusted according to measurement requirements. As long as the window did not reach the end of the signal length, the PPG and ACC signals were averaged and normalized, followed by the application of DFT and normalization to both PPG and ACC signals. The PPG signal underwent Fourier transformation to identify the amplitude in its spectrum. The heart rate corresponding to the frequency with the largest value was considered the current heart rate. Since heart rate fluctuations occur within a specific range, the algorithm only needs to operate within a particular frequency interval. The heart rate of a normal adult during deep sleep is not lower than 60 bpm, and the exercise heart rate formula indicates that an adult's heart rate during exercise does not exceed 220 minus their age [24]. Therefore, we chose a heart rate range of 60–192 bpm, corresponding to a frequency range of 1–3.2 Hz. As altering the heart rate interval range does not impact the algorithm's structure but only affects the accuracy of heart rate calculation, the following analysis is based on the algorithm's results within the 60–192 bpm heart rate interval.

The primary causes of motion artifacts encompass the movement of the measured area and changes in the distance between the PPG signal acquisition equipment and the measured area, among others. Wiener filtering is generally employed to remove motion artifacts [25]. The Wiener filter is based on the premise that noise and the original signal are independent of each other, utilizing their correlation to extract the actual signal from the noisy observation according to the minimum mean square error criterion. However, when a PPG signal and an ACC signal share the same frequency, they can no longer be considered independent during that period, rendering the Wiener filter ineffective for such artifacts. In light of the Wiener filtering principle, this paper simplified the engineering approach by subtracting the DFT results of the magnitude of the three-axis accelerometer signal acceleration (X-axis, Y-axis, Z-axis) from the DFT results of the PPG signal. The calculation of the magnitude of the three-axis accelerometer signal. This is typically done by using Equation (1), where ax , ay and az are the acceleration measurements in the x , y and z directions, respectively. The frequency component with the largest amplitude was then selected as an estimate based on the threshold value rule, and the heart rate value was subsequently calculated. A sliding window of 25 points was employed, with calculations

repeated in a cyclical manner. This method enabled the generation of a heart rate curve and the determination of the accuracy rate.

$$magnitude = \sqrt{(ax)^2 + (ay)^2 + (az)^2} \quad (1)$$

2.3. Experiment Results

The accuracy of a sample was determined by the proportion of accurate sample values to the total sample values. This accuracy served as the direct evaluation criterion for the effectiveness of the algorithm, with higher accuracy indicating better performance. Out of the 100 samples, 88 achieved an accuracy rate above 90%, with 8 of these samples achieving a perfect accuracy rate of 100%. The lowest accuracy rate among these 88 samples was 90.18%, while the average accuracy rate was 96.66%. The remaining 12 samples had an accuracy rate lower than 90%.

An example of qualified samples is presented with the daily activities of participant 17 shown in Figure 4, which displays the heart rate comparison chart of the PPG-predicted heart rate and heart rate band. The trend of the two heart rate measurements is approximately the same. Additionally, the spectral of PPG and ACC are shown in Figure 5a, while Figure 5b shows the spectral difference between PPG and ACC. Typically, the PPG signal contains two frequency components with a large amplitude, which are reflected in the spectrum in the wave peak corresponding to the actual heart rate and the wave peak generated when the bracelet follows the arm movement. The latter peak is eliminated by subtracting the ACC spectrum, retaining only the wave peak at the actual heart rate, and the heart rate corresponding to this peak is the estimated heart rate.

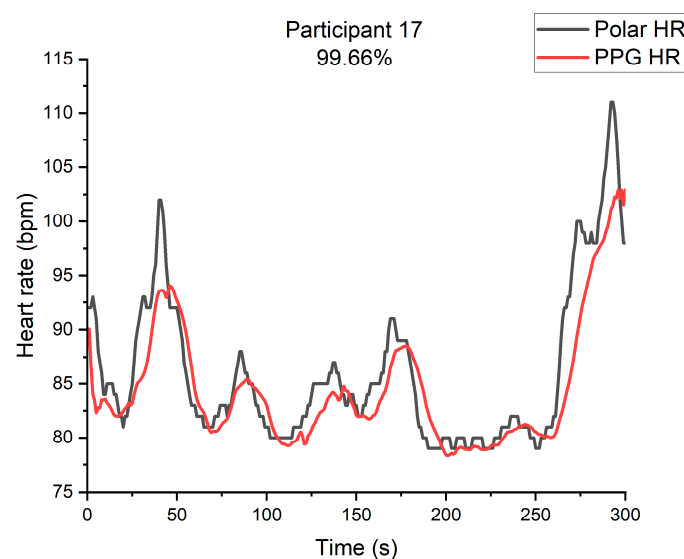


Figure 4. Participant 17's heart rate of PPG and heart rate band.

We also analyzed the unqualified samples. Apart from the samples that were unusable due to poor signal quality resulting from incorrect wearing, two samples showed PPG and ACC spectra overlapping at the actual heart rate. Figure 6 shows the comparison between the PPG-predicted heart rate and the heart rate from the heart rate band when participant 9 walked up and down stairs. The PPG-predicted heart rate could no longer follow the heart rate band. Figure 7a displays the spectral of PPG and ACC and Figure 7b shows the spectral difference between PPG and ACC. Figure 8 illustrates the comparison between the PPG-predicted heart rate and the heart rate from the heart rate band when participant 14 walked up and down stairs. The PPG-predicted heart rate could no longer follow the heart rate band. Figure 9a shows the spectral of PPG and ACC, and Figure 9b displays the spectral difference between PPG and ACC. The ACC signal contains low-frequency

components. The PPG and ACC spectra have wave peaks at the actual heart rate, and there is no wave peak at the actual heart rate after the two are subtracted. Consequently, the wave peak corresponding to the actual heart rate in the PPG spectrum is reduced as a motion artifact when the heart rate is not high. The algorithm takes a value far higher than the actual heart rate, and the accuracy of the heart rate measurement of participant 9 walking up and down stairs is 23.79%. The accuracy rate of the heart rate measurement of participant 14 is 61.56%. This error is due to the participant's acceleration coinciding with their heart rate during exercise. In our sample space, the frequency of this situation is 0.02. Although this is a low probability event, this problem cannot be avoided by evaluating the signal quality to determine whether to discard a piece of data before calculation. This problem is also a common occurrence in engineering, and therefore the impact on measurement accuracy is critical.

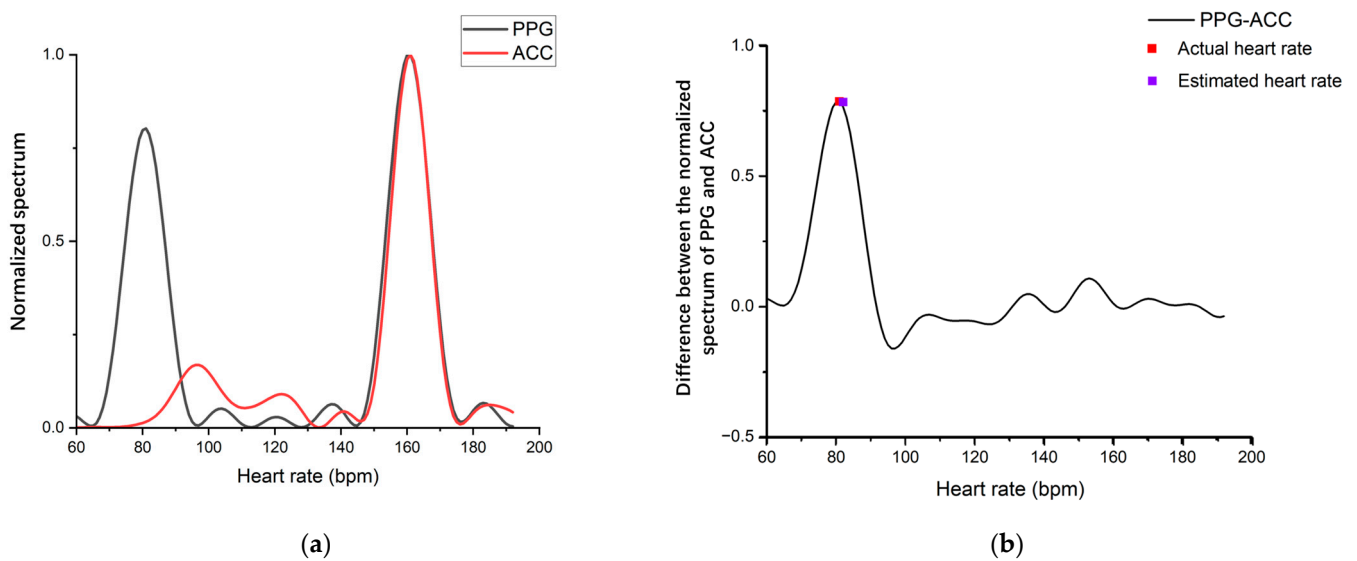


Figure 5. The spectral of participant 17. (a) The spectral of PPG and ACC; (b) Spectral difference between PPG and ACC.

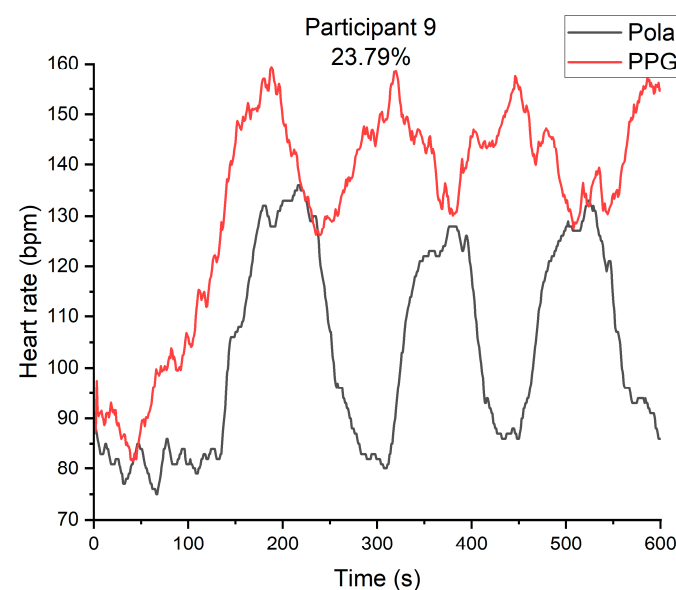


Figure 6. Participant 9's heart rate of PPG and heart rate band.

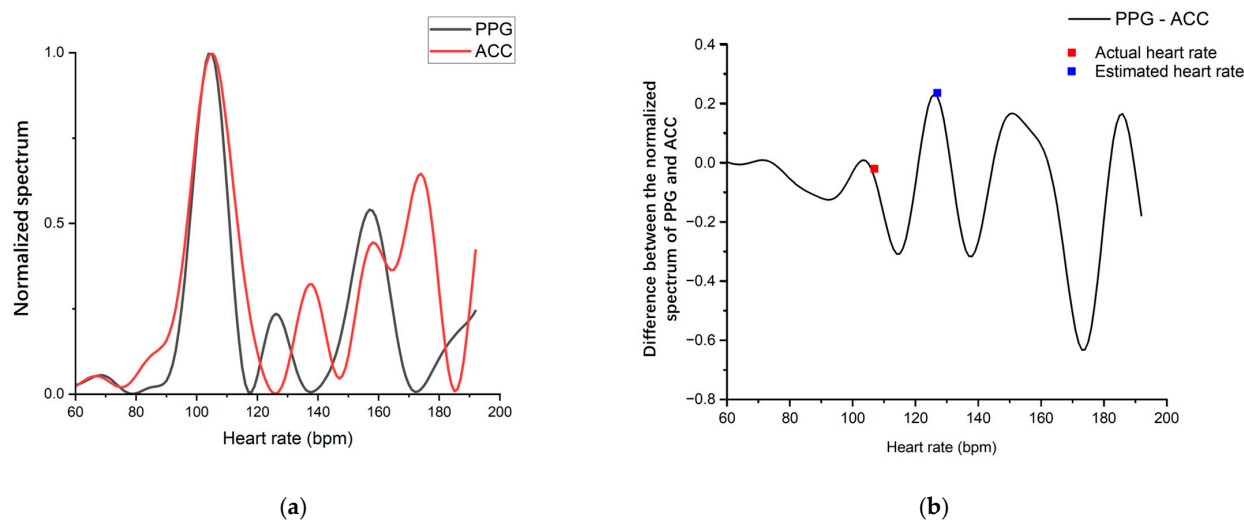


Figure 7. The spectral of participant 9. (a) The spectral of PPG and ACC; (b) Spectral difference between PPG and ACC.

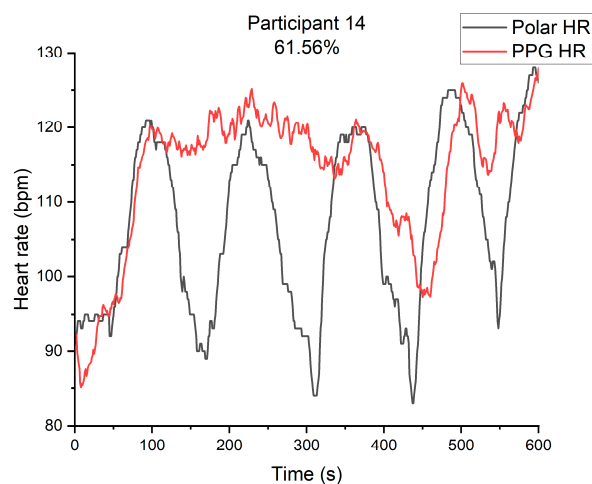


Figure 8. Participant 14's heart rate of PPG and heart rate band.

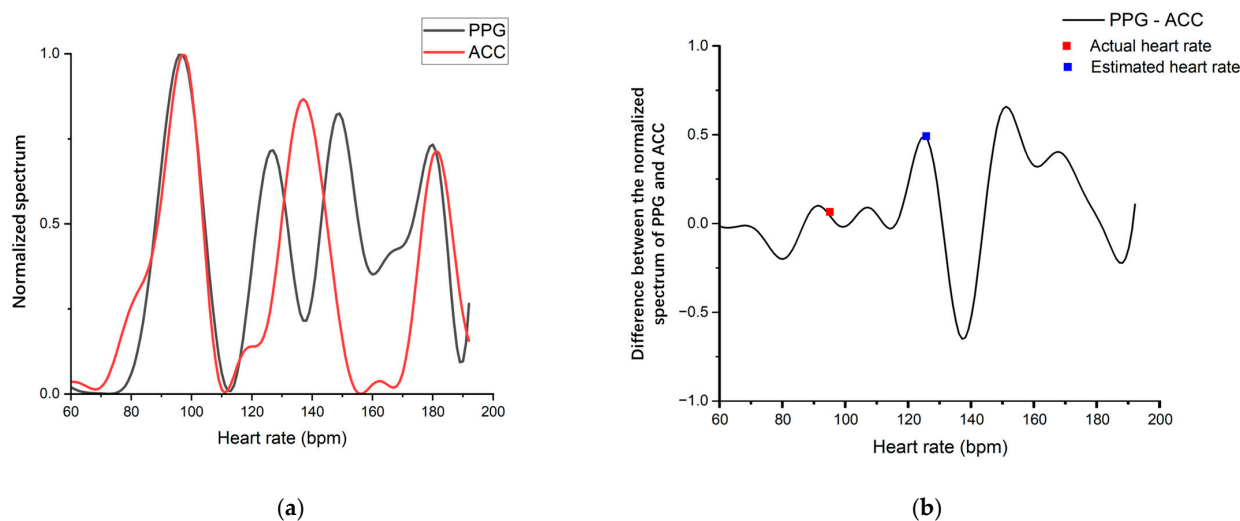


Figure 9. The spectral of participant 14. (a) The spectral of PPG and ACC; (b) Spectral difference between PPG and ACC.

In summary, while the traditional DFT algorithm has a certain accuracy in measuring heart rate, it fails to compute the correct heart rate when the PPG spectrum and ACC spectral overlap at the actual heart rate. Therefore, the algorithm needs to be enhanced to address the issues related to overlapping spectra.

3. Algorithm Improvement

3.1. Algorithm Improvement Architecture

During the heart rate extraction algorithm experiment using the sports bracelet's photoplethysmography on a group of individuals, a practical issue was discovered. The algorithm faces difficulty in resolving cases where the PPG signal spectrum and ACC signal spectrum exhibit peaks simultaneously at the actual heart rate. The algorithm eliminates the PPG spectrum peak at this point, considering it to be a motion artifact, leading to an incorrect estimated heart rate. To address this issue, the algorithm was improved to enhance accuracy. This study recruited a total of 20 participants, each of whom was assigned a unique sequential numerical identifier. The experimental dataset utilized for algorithm design comprised data collected from participants assigned odd-numbered identifiers, while the algorithm validation dataset comprised data collected from participants assigned even-numbered identifiers.

The flow chart for the improved heart rate calculation is presented in Figure 10. To improve the traditional algorithm's step of subtracting the DFT results of PPG and ACC, we first determine the spectral overlap by examining the morphological characteristics of PPG and ACC spectra. Following the detection of overlap, we incorporate the SSA algorithm, which does not rely on spectrum subtraction, to recalculate the current heart rate and remove motion artifacts.

Subtract the DFT results of PPG and ACC

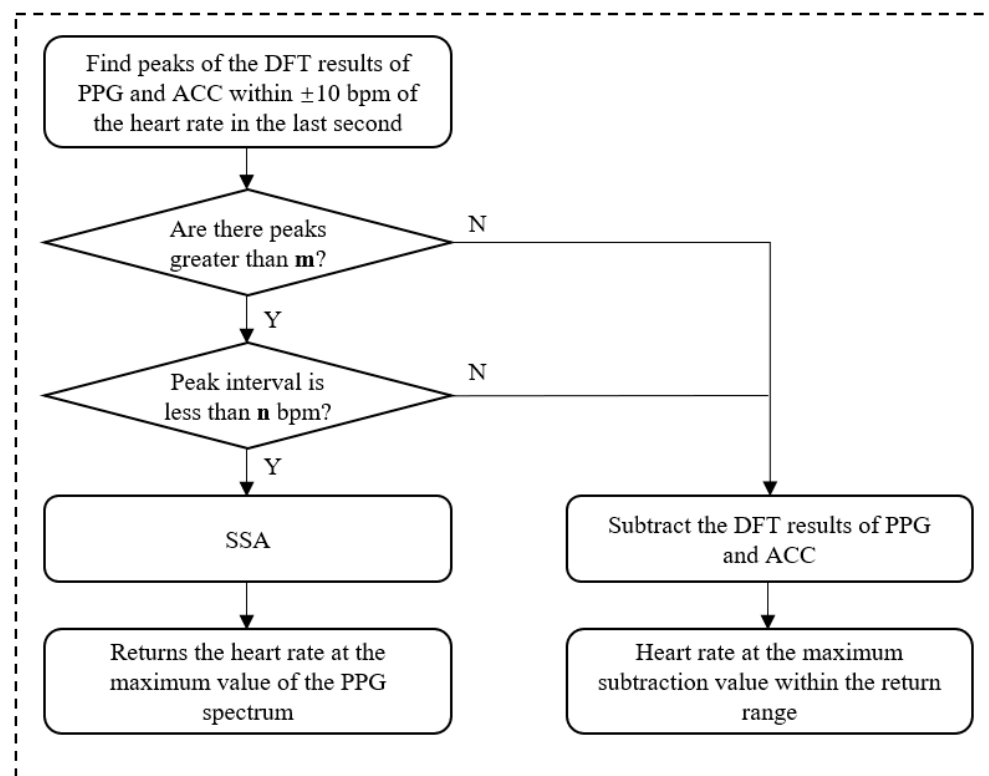


Figure 10. Algorithm improvement architecture.

To address the issue of PPG and ACC spectra overlapping at the heart rate, we first need to determine if it occurs. As the human heart rate does not change significantly within 1 s, the difference between the current heart rate and that of the previous second

should not exceed 10 bpm. Therefore, we only need to detect spectral overlap within the range of the previous heart rate ± 10 bpm. In the spectrum obtained from the Fourier transform, the amplitude of a peak represents the signal energy of the corresponding frequency component. The larger the peak amplitude, the greater the signal energy. In the normalized spectrum, when the peak amplitude is greater than a certain threshold m , the frequency corresponding to the peak amplitude is considered to be the main frequency component in the signal. In the 1–3.2 Hz range, the main frequency components of the PPG spectrum are the frequencies corresponding to cardiac pulsations and motion artifacts, and the main frequency components of the ACC spectrum are the frequencies corresponding to motion artifacts. To detect spectral overlap, we need to find n_1 and n_2 , where n_1 represents the heart rate value corresponding to the peak of the normalized PPG spectrum and n_2 represents the heart rate value corresponding to the peak of the normalized ACC spectrum. We calculate the difference of $|n_1 - n_2|$. Figure 11 showcases the spectra of participant 9 along with the corresponding parameters. If the difference is less than n bpm, the two maxima can be considered the same. In this case, the overlap occurs at this moment. After detecting spectral overlap, we require a new algorithm to calculate the current window heart rate, which is different from the original algorithm's method of removing motion artifacts. Therefore, we introduce the Singular Spectrum Analysis (SSA) algorithm.

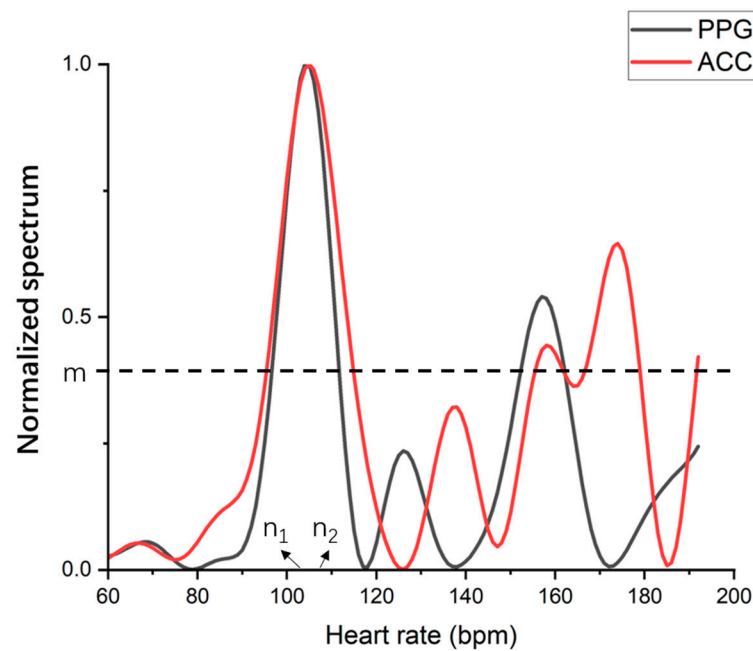


Figure 11. The spectra of participant 9 with corresponding parameters, where n_1 and n_2 are heart rates corresponding to peaks and m is the threshold of peaks.

SSA is a method of analyzing nonlinear time series by using matrix singular value decomposition (SVD) [26]. It constructs a trajectory matrix based on the observed time series and decomposes and reconstructs the trajectory matrix to extract signals representing different components of the original time series, including noise signals. The specific steps are embedding, SVD, grouping and reconstruction.

Embedding: map a time series $y = [y_1, y_2, \dots, y_M]$ of length M into an L -trajectory matrix Y of size $L \times K$ ($K = M - L + 1, L < M/2$),

$$Y = \begin{bmatrix} y_1 & y_2 & \cdots & y_K \\ y_2 & y_3 & \cdots & y_{K+1} \\ \vdots & \vdots & \ddots & \vdots \\ y_L & y_{L+1} & \cdots & y_M \end{bmatrix} \quad (2)$$

SVD: singular value decomposition of the matrix Y ,

$$Y = \sum_{i=1}^d Y_i = \sum_{i=1}^d \sigma_i u_i v_i^T, d = \min\{L, K\} \quad (3)$$

Grouping: divide Y_i into g groups of different linearly independent sub-matrices; each sub-matrix is the sum of Y_i within the group.

Reconstruction: reconstruct the grouped g sub-matrices into g time series of length M , then the original time series y can be expressed as the sum of the g time series of length M .

Based on the SSA algorithm, the PPG signal after motion artifact removal is obtained by eliminating the time series related to ACC from the PPG signal, followed by DFT to find the peak for heart rate calculation. Unlike the traditional algorithm, this approach does not require the subtraction of the two frequency domain signals, making it suitable for heart rate calculation when frequency spectra overlap.

3.2. Experiment Results

Based on the findings from the experimental dataset, we determined the value of m to be 0.4 and the value of n to be 3. In this scenario, the average accuracy of the samples without spectral overlap in the experimental dataset reached 95.95%, aligning with the algorithm results delineated in Chapter 2. Significantly, the accuracy of the samples exhibiting spectral overlap improved from 23.79% to 61.40%. The experimental results for participant 9 walking up and down stairs are presented in Figure 12. Figure 12a shows the accuracy rate obtained using the traditional algorithm, while Figure 12b shows the accuracy rate of the heart rate calculation result of the improved algorithm for samples with spectral overlap.

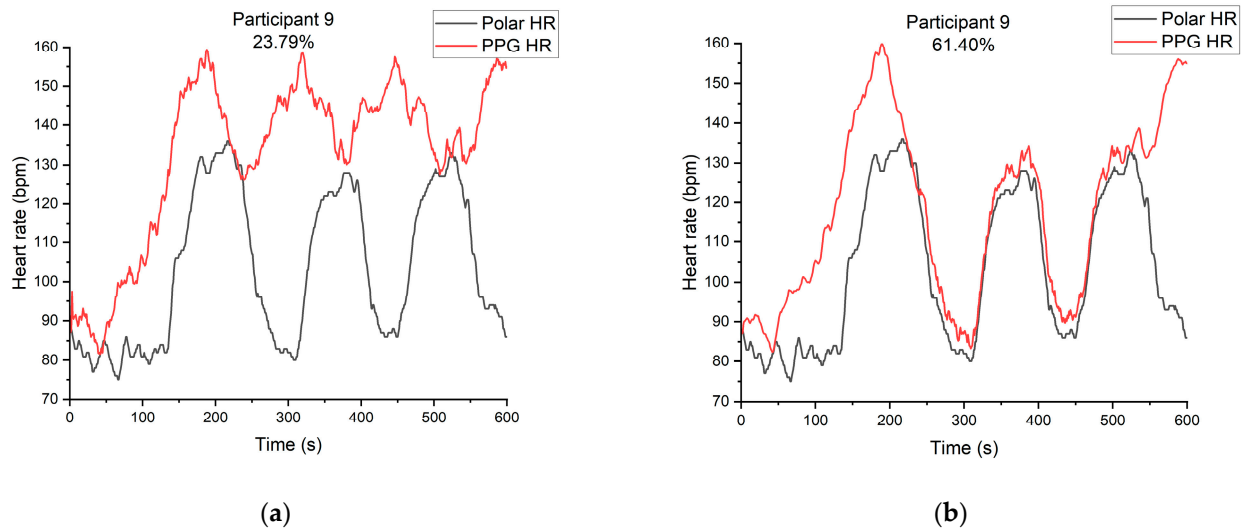


Figure 12. The experiment results for participant 9 walking up and down stairs. (a) The accuracy rate obtained using the traditional algorithm; (b) The accuracy rate obtained using the improved algorithm.

For participant 9 when walking up and down stairs, the spectral overlap phenomenon occurred. The accuracy rate of the original algorithm in this sample was 23.79%. After introducing the spectral overlap judgment and the SSA algorithm, the algorithm's accuracy rate improved to 61.40%, which is an improvement of 37.61%.

Moreover, after manually checking the PPG and ACC spectra of each point, it was found that there were 273 points in this sample with spectral overlap. The SSA algorithm was employed 269 times, and the judgment accuracy was 98.50%. Furthermore, in other samples without spectral overlap, the SSA algorithm was only applied 11 times in one

sample, and the number of uses was in the single digits for the rest of the samples, which demonstrates the accuracy of the spectral overlap judgment.

To validate the accuracy of the improved algorithm, we applied it to the validation dataset. The average accuracy of the samples without spectral overlap in the validation dataset reached 97.37%, which aligns with the algorithm outcomes discussed in Section 2. For the samples exhibiting spectral overlap, the accuracy notably increased from 61.56% to 80.57%. The experiment results for participant 14, walking up and down stairs, are presented in Figure 13. The accuracy rate obtained using the traditional algorithm is displayed in Figure 13a, while the accuracy rate of the improved algorithm for samples with spectral overlap is shown in Figure 13b.

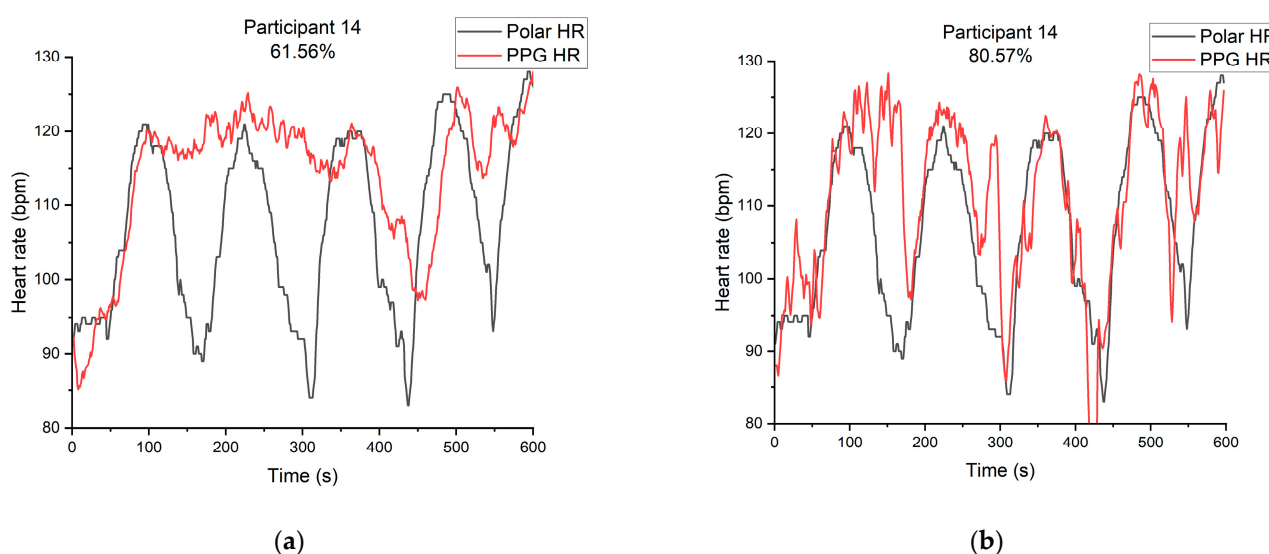


Figure 13. The experiment results for participant 14 walking up and down stairs. (a) The accuracy rate obtained using the traditional algorithm; (b) The accuracy rate obtained via the improved algorithm.

The spectral overlap phenomenon appeared in the sample for participant 14 walking up and down stairs. The original algorithm achieved an accuracy rate of 61.56% for calculating the heart rate in this sample. After introducing the spectral overlap judgment and the SSA algorithm, the calculated accuracy rate improved to 80.57%, showing an improvement of 19.01%.

Furthermore, upon examining the PPG spectrum and ACC spectrum of each point one by one, it was found that 125 points in this sample had spectral overlap, and the SSA algorithm was used 116 times with a spectral overlap judgment accuracy rate of 92.80%. Meanwhile, in samples without spectral overlap, the SSA algorithm was called no more than 11 times, demonstrating the accuracy of spectral overlap judgment.

This paper addresses the issue of inaccurate heart rate calculation caused by overlapping PPG and ACC spectra at the actual heart rate, by proposing an improved algorithm. The algorithm detects spectral overlap and utilizes the SSA algorithm to calculate the heart rate at the current moment without relying on spectrum subtraction to remove motion artifacts. The experimental results show that the proposed algorithm improves the accuracy of heart rate calculation by at least 19.01% compared to the traditional DFT method. The success of this algorithm in solving the issues in the original algorithm has been demonstrated.

4. Discussion

The traditional heart rate extraction algorithm subtracts the PPG spectrum from the ACC spectrum to remove motion artifacts. However, when both the normalized PPG spectrum and ACC spectrum have peaks at the actual heart rate, the traditional algorithm eliminates the peak at the actual heart rate, considering it a motion artifact. To

address this issue, we propose an improved algorithm that analyzes the individual signal characteristics. We partitioned the data into two distinct datasets: an experimental dataset and a validation dataset. Subsequently, we conducted an analysis of the results derived from the experimental dataset. Firstly, we judge the spectral overlap according to the morphological characteristics of the PPG and ACC spectra. We find the local maximums of the normalized PPG and ACC spectra in the range to detect the overlap. If local maximums greater than 0.4 are found in the normalized PPG and ACC spectra, respectively, we calculate the difference between the PPG local maximums and the ACC local maximums. If the difference is less than 3 bpm, the overlap is detected. Then, we introduce the SSA algorithm to recalculate the heart rate at the current moment when overlap is detected. The SSA algorithm removes motion artifacts by decomposing and reconstructing the PPG signal in the time domain, removing the time series related to ACC. DFT and peak search are directly performed on the reconstructed signal. The improved algorithm was applied to participant 9, achieving a spectral overlap judgment accuracy of 98.5%, and the accuracy increased from 23.79% to 61.40%, improving by 37.61%. To validate the accuracy of the improved algorithm, we applied it to the validation dataset. The improved algorithm was also tested on participant 14, achieving a spectral overlap judgment accuracy of 92.8%, and the accuracy increased from 61.65% to 80.57%, improving by 19.01%.

Table 2 presents a comparison of the proposed algorithm with peak detection of the PPG signal, the DFT algorithm and the TROIKA framework, which employs the SSA signal decomposition approach, in terms of accuracy, algorithmic complexity and floating-point operations (FLOPs). The peak detection algorithm, which counts the number of main peaks of the PPG signal in one minute, has the lowest algorithmic complexity and FLOPs. However, its accuracy is much lower than that of the other three algorithms, rendering it not commonly used for heart rate estimation. The accuracy of samples without spectral overlap is determined by computing the average accuracy of 10 randomly selected samples from the validation dataset. In this case, the accuracy of the proposed algorithm is 96.66%, which is the same as that of the DFT algorithm and only 0.51% lower than that of the TROIKA framework. In terms of algorithmic complexity and FLOPs, the two terms of the proposed algorithm are significantly lower than those of the TROIKA framework. In conclusion, the proposed algorithm solves the problem of spectral overlap that the DFT algorithm cannot handle, and its accuracy is close to that of the TROIKA framework. Moreover, its algorithmic complexity is within an acceptable range, making it much easier to use in wearable devices than the TROIKA framework.

Table 2. Comparison on performance indicators of the proposed algorithm with existing algorithms.

Algorithm	Peak Detection	DFT	TROIKA	Proposed Algorithm
Accuracy (with spectral overlap)	51.95%	61.56%	82.88%	80.57%
Accuracy (without spectral overlap)	82.70%	96.66%	97.17%	96.66%
Algorithm complexity	N	$N \times \log N$	$3N^3$	$3pN^3 + (1-p)N \times \log N$
FLOPs	$3N - 4$	$8N \times \log_2 N$	$3N^3 + (13 + \log_2 N) \times N^2 + 55N$	$8pN \log_2 N + 3pN^3 + (13p + p \log_2 N) \times N^2 + 55pN$

The algorithmic complexity and FLOPs of the proposed algorithm are given by $p \times \text{TROIKA} + (1-p) \times \text{DFT}$ where p is the probability of spectral overlap. In this study, spectral overlap is detected in two of the one hundred samples, so $p = 0.02$ in the table.

In addition to the algorithms discussed above, current artificial intelligence and machine learning techniques are extensively used in heart rate extraction from PPG and ACC data, such as Convolutional-Recurrent Neural Networks (C-RNN) [27], PPG-NeXt network [28] and Support Vector Machine (SVM) [29]. These methodologies, although possessing significant potential, require a substantial amount of annotated data for training. Their accuracy is also often limited by the dataset, making it challenging to obtain sufficient

data for training in certain uncommon scenarios, such as the spectral overlap problem mentioned earlier. Simultaneously, complex AI models require considerable computational resources, making them unsuitable for deployment on wearable devices.

The experimental results demonstrate that the improved algorithm effectively addresses the issue of incorrect heart rate estimation due to PPG-ACC spectral overlap, resulting in improved accuracy. However, the algorithm does increase computational complexity due to the matrix operations involved in the SSA algorithm. Nonetheless, as the SSA algorithm is only applied when spectral overlap occurs, which is a low-probability event, it does not place excessive computational burden on the overall measurement system.

In future research, we will continue to recruit participants to collect more data and also consider other factors that may be present during the experiment to make our algorithm more universal and further enhance its accuracy. We will also investigate the application of Artificial Intelligence-based techniques to assist in the determination of optimal thresholds. Additionally, we plan to optimize the proposed algorithm at the hardware level to ensure compatibility with wearable devices and minimize power consumption.

5. Conclusions

The proposed algorithm is an improvement over traditional heart rate extraction algorithms, as it effectively tackles the issue of inaccurate heart rate computation when the PPG and ACC spectra overlap. Initially, the algorithm identifies spectral overlap based on the morphological characteristics of the PPG and ACC spectra. When overlap is detected, the SSA algorithm calculates the heart rate without relying on spectrum subtraction to eliminate motion artifacts. In the experimental dataset, the results indicate that the enhanced algorithm boosts heart rate estimation accuracy, with a 98.5% accuracy rate in judging spectral overlap for participant 9 and an accuracy rate increase from 23.79% to 61.40% for this participant, yielding an improvement of 37.61%. In the validation dataset, the accuracy rate of spectral overlap for participant 14 is 92.8%, and the accuracy rate rises from 61.65% to 80.57%, achieving an improvement of 19.01%. The proposed algorithm effectively addresses the challenges of overlapping spectra and motion artifacts in conventional algorithms, resulting in substantial enhancements in heart rate extraction accuracy.

Author Contributions: Conceptualization, M.L.; methodology, B.R. and Z.W.; software, Z.W. and K.M.; validation, B.R., K.M., Z.W. and Y.Z.; formal analysis, B.R. and Z.W.; investigation, K.M. and Z.W.; resources, B.R. and Z.W.; data curation, B.R. and Z.W.; writing—original draft preparation, B.R.; writing—review and editing, B.R., K.M. and Z.W.; visualization, B.R.; supervision, K.M. and M.L.; project administration, M.L.; funding acquisition, M.L. All authors have read and agreed to the published version of the manuscript.

Funding: This research received no external funding.

Data Availability Statement: The data are available upon request.

Conflicts of Interest: The authors declare no conflict of interest.

References

- Guo, Y.; Lane, D.A.; Wang, L.; Zhang, H.; Wang, H.; Zhang, W.; Wen, J.; Xing, Y.; Wu, F.; Xia, Y.; et al. Mobile Health Technology to Improve Care for Patients with Atrial Fibrillation. *J. Am. Coll. Cardiol.* **2020**, *75*, 1523–1534. [[CrossRef](#)] [[PubMed](#)]
- Pankaj; Kumar, A.; Komaragiri, R.; Kumar, M. A Review on Computation Methods Used in Photoplethysmography Signal Analysis for Heart Rate Estimation. *Arch. Comput. Methods Eng.* **2021**, *29*, 921–940. [[CrossRef](#)]
- Ray, D.; Collins, T.; Woolley, S.; Ponnapalli, P. A Review of Wearable Multi-wavelength Photoplethysmography. *IEEE Rev. Biomed. Eng.* **2021**, *16*, 136–151. [[CrossRef](#)] [[PubMed](#)]
- Fine, J.; Branan, K.L.; Rodriguez, A.J.; Boonya-Ananta, T.; Ajmal; Ramella-Roman, J.C.; McShane, M.J.; Cote, G.L. Sources of Inaccuracy in Photoplethysmography for Continuous Cardiovascular Monitoring. *Biosensors* **2021**, *11*, 126. [[CrossRef](#)]
- Salehizadeh, S.M.; Dao, D.; Bolkhovsky, J.; Cho, C.; Mendelson, Y.; Chon, K.H. A Novel Time-Varying Spectral Filtering Algorithm for Reconstruction of Motion Artifact Corrupted Heart Rate Signals during Intense Physical Activities Using a Wearable Photoplethysmogram Sensor. *Sensors* **2016**, *16*, 10. [[CrossRef](#)]
- Ismail, S.; Akram, U.; Siddiqi, I. Heart rate tracking in photoplethysmography signals affected by motion artifacts: A review. *EURASIP J. Adv. Signal Process.* **2021**, *2021*, 5. [[CrossRef](#)]

7. Liu, H.; Allen, J.; Khalid, S.G.; Chen, F.; Zheng, D. Filtering-induced time shifts in photoplethysmography pulse features measured at different body sites: The importance of filter definition and standardization. *Physiol. Meas.* **2021**, *42*, 074001. [\[CrossRef\]](#)
8. Allen, J.; Murray, A. Effects of filtering on multisite photoplethysmography pulse waveform characteristics. In Proceedings of the Computers in Cardiology, Chicago, IL, USA, 19–22 September 2004; pp. 485–488.
9. Loh, H.W.; Xu, S.; Faust, O.; Ooi, C.P.; Barua, P.D.; Chakraborty, S.; Tan, R.-S.; Molinari, F.; Acharya, U.R. Application of photoplethysmography signals for healthcare systems: An in-depth review. *Comput. Methods Programs Biomed.* **2022**, *216*, 106677. [\[CrossRef\]](#)
10. Allen, J.; Liu, H.; Iqbal, S.; Zheng, D.; Stansby, G. Deep learning-based photoplethysmography classification for peripheral arterial disease detection: A proof-of-concept study. *Physiol. Meas.* **2021**, *42*, 054002. [\[CrossRef\]](#)
11. Kotzen, K.; Charlton, P.H.; Salabi, S.; Amar, L.; Landesberg, A.; Behar, J.A. SleepPPG-Net: A deep learning algorithm for robust sleep staging from continuous photoplethysmography. *IEEE J. Biomed. Health Inform.* **2022**, *27*, 924–932. [\[CrossRef\]](#)
12. Khan, E.; Al Hossain, F.; Uddin, S.Z.; Alam, S.K.; Hasan, M.K. A Robust Heart Rate Monitoring Scheme Using Photoplethysmographic Signals Corrupted by Intense Motion Artifacts. *IEEE Trans. Biomed. Eng.* **2016**, *63*, 550–562. [\[CrossRef\]](#) [\[PubMed\]](#)
13. Ye, Y.L.; Cheng, Y.F.; He, W.W.; Hou, M.S.; Zhang, Z.L. Combining Nonlinear Adaptive Filtering and Signal Decomposition for Motion Artifact Removal in Wearable Photoplethysmography. *IEEE Sens. J.* **2016**, *16*, 7133–7141. [\[CrossRef\]](#)
14. Fukushima, H.; Kawanaka, H.; Bhuiyan, M.S.; Oguri, K. Estimating Heart Rate using Wrist-type Photoplethysmography and Acceleration sensor while running. In Proceedings of the 34th Annual International Conference of the IEEE Engineering-in-Medicine-and-Biology-Society (EMBS), San Diego, CA, USA, 28 August–1 September 2012; pp. 2901–2904.
15. Chen, G.; Imtiaz, S.A.; Aguilar-Pelaez, E.; Rodriguez-Villegas, E. Algorithm for heart rate extraction in a novel wearable acoustic sensor. *Healthc. Technol. Lett.* **2015**, *2*, 28–33. [\[CrossRef\]](#) [\[PubMed\]](#)
16. Salehizadeh, S.M.A.; Dao, D.K.; Chong, J.W.; McManus, D.; Darling, C.; Mendelson, Y.; Chon, K.H. Photoplethysmograph Signal Reconstruction based on a Novel Motion Artifact Detection-Reduction Approach. Part II: Motion and Noise Artifact Removal. *Ann. Biomed. Eng.* **2014**, *42*, 2251–2263. [\[CrossRef\]](#) [\[PubMed\]](#)
17. Orphanidou, C.; Orphanidou, C. Quality Assessment for the photoplethysmogram (PPG). In *Signal Quality Assessment in Physiological Monitoring: State of the Art and Practical Considerations*; Springer: Cham, Switzerland, 2018; pp. 41–63.
18. Khalid, S.G.; Ali, S.M.; Liu, H.; Qurashi, A.G.; Ali, U. Photoplethysmography temporal marker-based machine learning classifier for anesthesia drug detection. *Med. Biol. Eng. Comput.* **2022**, *60*, 3057–3068. [\[CrossRef\]](#) [\[PubMed\]](#)
19. Karavaev, A.S.; Borovik, A.S.; Borovkova, E.I.; Orlova, E.A.; Simonyan, M.A.; Ponomarenko, V.I.; Skazkina, V.V.; Gridnev, V.I.; Bezruchko, B.P.; Prokhorov, M.D. Low-frequency component of photoplethysmogram reflects the autonomic control of blood pressure. *Biophys. J.* **2021**, *120*, 2657–2664. [\[CrossRef\]](#) [\[PubMed\]](#)
20. Liu, H.; Chen, F.; Hartmann, V.; Khalid, S.G.; Hughes, S.; Zheng, D. Comparison of different modulations of photoplethysmography in extracting respiratory rate: From a physiological perspective. *Physiol. Meas.* **2020**, *41*, 094001. [\[CrossRef\]](#) [\[PubMed\]](#)
21. Maeda, Y.; Sekine, M.; Tamura, T. Relationship between measurement site and motion artifacts in wearable reflected photoplethysmography. *J. Med. Syst.* **2011**, *35*, 969–976. [\[CrossRef\]](#) [\[PubMed\]](#)
22. Hughes, S.; Liu, H.; Zheng, D. Influences of sensor placement site and subject posture on measurement of respiratory frequency using triaxial accelerometers. *Front. Physiol.* **2020**, *11*, 823. [\[CrossRef\]](#)
23. Saquib, N.; Papon, M.T.I.; Ahmad, I.; Rahman, A. Measurement of Heart Rate Using Photoplethysmography. In Proceedings of the Networking Systems and Security NSysS International Conference, Dhaka, Bangladesh, 5–7 January 2015; pp. 158–163.
24. Robergs, R.A.; Landwehr, R. The surprising history of the “HRmax= 220-age” equation. *J. Exerc. Physiol.* **2002**, *5*, 1–10.
25. Temko, A. Accurate Heart Rate Monitoring during Physical Exercises Using PPG. *IEEE Trans. Biomed. Eng.* **2017**, *64*, 2016–2024. [\[CrossRef\]](#) [\[PubMed\]](#)
26. Zhang, Z.L.; Pi, Z.Y.; Liu, B.Y. TROIKA: A General Framework for Heart Rate Monitoring Using Wrist-Type Photoplethysmographic Signals during Intensive Physical Exercise. *IEEE Trans. Biomed. Eng.* **2015**, *62*, 522–531. [\[CrossRef\]](#) [\[PubMed\]](#)
27. Ismail, S.; Siddiqi, I.; Akram, U. Heart rate estimation in PPG signals using Convolutional-Recurrent Regressor. *Comput. Biol. Med.* **2022**, *145*, 105470. [\[CrossRef\]](#)
28. Hnoohom, N.; Mekruksavanich, S.; Jitpattanakul, A. Physical Activity Recognition Based on Deep Learning Using Photoplethysmography and Wearable Inertial Sensors. *Electronics* **2023**, *12*, 693. [\[CrossRef\]](#)
29. Moscato, S.; Lo Giudice, S.; Massaro, G.; Chiari, L. Wrist Photoplethysmography Signal Quality Assessment for Reliable Heart Rate Estimate and Morphological Analysis. *Sensors* **2022**, *22*, 5831. [\[CrossRef\]](#)

Disclaimer/Publisher’s Note: The statements, opinions and data contained in all publications are solely those of the individual author(s) and contributor(s) and not of MDPI and/or the editor(s). MDPI and/or the editor(s) disclaim responsibility for any injury to people or property resulting from any ideas, methods, instructions or products referred to in the content.